JACS
JOURNAL OF THE AMERICAN CHEMICAL SOCIETY
Article
pubs.acs.org/JACS

A New Mixed Halide, $Cs_2HgI_2Cl_2$: Molecular Engineering for a New Nonlinear Optical Material in the Infrared Region

Gang Zhang,[†,⊥] Yanjun Li,[†,⊥] Kui Jiang,[†] Huiyi Zeng,[§] Tao Liu,[†] Xingguo Chen,[†] Jingui Qin,*[,†] Zheshuai Lin,*[,‡] Peizhen Fu,[‡] Yicheng Wu,[‡] and Chuangtian Chen[‡]

[†]Department of Chemistry, Wuhan University, Wuhan 430072, China

[‡]Beijing Center for Crystal R & D, Technical Institute of Physics and Chemistry, Chinese Academy of Sciences, Beijing 100190, China

[§]State Key Laboratory of Structural Chemistry, Fujian Institute of Research on the Structure of Matter, Chinese Academy of Sciences, Fuzhou 350002, China

Supporting Information

ABSTRACT: A new mixed halide, $Cs_2HgI_2Cl_2$, which contains the highly polar tetrahedron of anion $(HgI_2Cl_2)^{2-}$, has been designed and synthesized by reaction in solution. In its single crystal, the isolated $(HgCl_2I_2)^{2-}$ groups are arranged to form chains. The chains are then further connected into a three-dimensional framework through the Cs atoms that occupy the empty spaces surrounded by halide atoms. All the polar $(HgCl_2I_2)^{2-}$ groups align in such a way that gives a net polarization, leading it to show a phase matchable second harmonic generation (SHG) effect as strong as that of KH_2PO_4 (KDP) based on the powder SHG measurement. It also displays excellent transparency in the range of 0.4−41 μm with relatively high thermal stability. A preliminary measurement indicates that its laser-induced damage threshold is about 83 MW/cm^2, about twice that of $AgGaS_2$. This study demonstrates that $Cs_2HgI_2Cl_2$ is a promising nonlinear optical material in the infrared region.

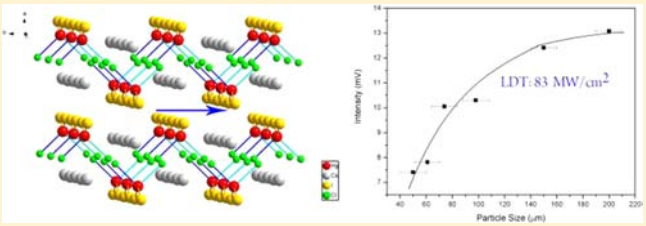

INTRODUCTION

Second-order nonlinear optical (NLO) materials have attracted much attention owing to their uses in laser frequency conversion, optical parameter oscillators (OPOs), and optical communication.[1,2] This resulted in the development of many important NLO crystals used in the UV and visible regions, including β-BaB_2O_4 (BBO),[3] LiB_3O_5 (LBO),[4] KH_2PO_4 (KDP),[5] $KTiOPO_4$ (KTP),[6] and $LiNbO_3$ (LN).[7] On the other hand, the known NLO crystals in the infrared (IR) region such as $AgGaS_2$[8,9] $AgGaSe_2$,[10] and $ZnGeP_2$[11] have suffered from some shortcomings including the difficulty to grow high quality crystals and the low laser damage threshold (LDT). In particular, the latter became the main obstacle for their applications. So the issue of how to improve the performance of IR NLO crystals has been focused on in the last two decades and become one of the great challenges in this field.[12] The first approach is to adapt new techniques for crystal growth so as to improve the quality of the crystals. A good example is $ZnGeP_2$ whose LDT has been improved by use of a new crystal growth method.[13,14] The second approach by many research groups is to modify the composite metal elements of existing IR crystals, and some new materials such as $LiInS_2$[15] and $BaGa_4S_7$[16] showed improved LDT.

The exact mechanism for laser damage of a crystal is not fully clear yet; however it has been normally accepted that strong optical absorption of the materials will cause thermal and electronic effects and finally lead to laser damage.[17] It is interesting to note that so far most commercialized IR NLO crystals are chalcogenides. It seems reasonable to propose that the small band gaps of the current semiconductive IR NLO crystals are the most important intrinsic reason for the laser damage. Nevertheless, compounds with large band gaps usually exhibit small NLO coefficients.[18] It is necessary to undertake careful molecular engineering to create the subtle balance of the above-mentioned conflicting factors so as to search for the new IR NLO crystals with excellent comprehensive performance. By considering this issue, we started a new approach at the end of the last century to search for new IR NLO crystals from the halides since they normally exhibit large band gaps and there are diverse choices from four halogen elements for composing an enormous number of halide compounds with diverse structural motifs so that it is possible to find suitable candidates from halides with excellent comprehensive properties, including large NLO effects, high LDT, and wide transparent window in the IR region among the others. Some new potential IR NLO materials such as $CsGeCl_3$,[19] $CsCdBr_3$,[20] $HgBr_2$,[21] and $NaSb_3F_{10}$[22] have been developed in this regard. In addition to the above approach for halides, another new approach is searching among oxides, another category of the compounds

Received: April 18, 2012
Published: August 15, 2012

   dx.doi.org/10.1021/ja3037299 | J. Am. Chem. Soc. 2012, 134, 14818−14822

with large band gaps. To be useful in the IR region, the elements that form the bonds with the oxygen atom are those with heavy atomic mass, such as iodine and tellurium. Some good results were also obtained.[23−31]

Recently, we have designed a mixed halide, $Cs_2HgI_2Cl_2$, according to the following considerations: (1) coexistence of two types of halide elements may increase the anisotropy and the polarity of the anionic group, $[HgI_2Cl_2]^{2-}$ (which is the NLO active unit of the compound), and enhance the possibility of overall NLO effects; (2) mercury is a heavy element, and the mercury−halide bonds will exhibit a wide window of infrared absorption; (3) the mercury(II) cation of d^{10} electronic configuration does not exhibit d−d excitation, which normally leads to small band gaps; (4) bonds between mercury and a halide are normally strong and will exhibit high stability; (5) the crystal can be synthesized and grown in solution, and the ionic character of $[Cs^+]_2[HgI_2Cl_2]^{2-}$ would benefit the crystal growth habit.

In this paper, we report the synthesis, crystal structure, and NLO properties of the new mixed-halide compound, $Cs_2HgI_2Cl_2$. It shows a powder second harmonic generation (SHG) property similar to that of KH_2PO_4 (KDP). In comparison with many commercial IR NLO crystals, $Cs_2HgI_2Cl_2$ exhibits a much higher laser-induced damage threshold (about 83 MW/cm^2). It also shows a wide transmission window in the IR range (up to 41 μm) and relatively high thermal stability. This is the first work to demonstrate that the mixed halide might be an excellent alternative for new NLO material in the IR region.

EXPERIMENTAL SECTION

Reagents. All starting materials were analytical grade from commercial sources. HgI_2, CsCl, and acetone were purchased from Sinopharm and used without further treatment.

Synthesis. The compound $Cs_2HgI_2Cl_2$ can be synthesized by conventional solution reaction. Stoichiometric amounts of CsCl (5.0508 g, 30 mmol) and HgI_2 (6.8160 g, 15 mmol) were carefully dissolved in 40 mL of acetone. The mixture was stirred at 45 °C for 24 h. The yellow solution was filtered and slowly cooled and then kept at 4 °C in a refrigerator. After 20 days, some pale yellow stick-shaped crystals appeared in the bottom of the flask. The pale yellow stick-shaped crystals were filtered and carefully washed with cool acetone. Colorless stick-shaped crystals of $Cs_2HgCl_2I_2$ were obtained (a photograph of a crystal is shown in Figure S2 in the Supporting Information).

Single-Crystal Structure Determinations. A single crystal of $Cs_2HgI_2Cl_2$ with dimensions of ca. 0.12 × 0.10 × 0.10 mm^3 was selected and used for the single-crystal diffraction experiment. Data sets were collected using a Bruker SMART APEX diffractometer equipped with a CCD detector (graphite-monochromated Mo Kα radiation, λ = 0.71073 Å) at 296(2) K. Data set reduction and integration were performed using the software package *SAINT PLUS*.[32] The crystal structure is solved by direct methods and refined using the *SHELXTL 97* software package.[33] Single-crystal data collection, cell parameters, and basic information for $Cs_2HgI_2Cl_2$ are summarized in Tables 1 and 2.

Powder X-ray Diffraction. X-ray powder diffraction (XRD) patterns of polycrystalline material were collected using a Bruker D8 Advanced diffractometer with Cu Kα_1 radiation (λ = 1.54186 Å) in the range of 10°−80° (2θ) at a scanning rate of 4°/min. The phase purity was checked, and no impurities were observed. The powder XRD patterns for $Cs_2HgI_2Cl_2$ obtained from solution reaction showed good agreement with the calculated XRD patterns from the single-crystal models (see Figure S1 in the Supporting Information).

Infrared Spectrum, Raman Spectrum, and UV−Vis Diffuse Reflectance Spectrum. The optical transmission spectrum in the mid-IR region was run on a NICOLET 5700 Fourier-transformed infrared (FTIR) spectrophotometer in the 4000−700 cm^{-1} region (2.5−14 μm) using the attenuated total reflection (ATR) technique with a germanium crystal. The Raman scattering spectrum in the 800−100 cm^{-1} region (12.5−100 μm) was carried out using a Renishaw RM 1000 laser confocal Raman microspectrometer at room temperature. The 514.5 nm line of an Ar-ion laser was used for excitation. The ATR-FTIR spectrum and the Raman spectrum were performed on $Cs_2HgCl_2I_2$ crystal. The UV−vis absorption spectrum was performed on a Varian Cary 5000 UV−vis−NIR spectrophotometer in the region 200−800 nm. A $BaSO_4$ plate was used as the standard (100% reflectance), on which the finely ground samples from the crystals were coated. The absorption spectrum was calculated from the reflectance spectra using the Kubelka−Munk function: $a/S = (1 - R)^2/(2R)$,[34] where a is the absorption coefficient, S is the scattering coefficient, and R is the reflectance.

NLO Property and LDT Measurements. The NLO efficiencies of the samples were investigated using a Kurtz−Perry powder technique.[35] A pulsed Q-switched Nd:YAG laser was utilized to generate fundamental 1064 nm light with a pulse width of 10 ns. Microcrystalline KDP served as the standard. Laser-induced damage test was performed[21,22] on very small crystalline samples without any pretreatment, with 10 Hz focused laser pulses emitted by the other laser source (1064 nm, 5 ns). The energy of each pulse was measured to be about 160 mJ. An optical concave lens was used to adjust the diameter of the laser beam to obtain different intensity. The samples

Table 1. Crystal Data and Structure Refinement for $Cs_2HgI_2Cl_2$[a]

empirical formula	$Cs_2HgI_2Cl_2$
formula weight	791.11
temp, K	296(2)
wavelength, Å	0.71073
cryst syst	monoclinic
space group	$P2_1$ (No. 4)
a, Å	8.0095(12)
b, Å	7.7557(12)
c, Å	9.8426(14)
α, deg	90
β, deg	108.160(2)
γ, deg	90
vol, Å^3	580.96(15)
Z	2
d_{calcd}, mg/m^3	4.522
abs coeff, mm^{-1}	25.123
F(000)	660
cryst size, mm^3	0.12 × 0.10 × 0.10
reflns collected	3243
indep reflns	2781 [R (int) = 0.0293]
GOF on F^2	1.123
R_1, wR_1 [$I > 2\sigma(I)$]	0.0350, 0.0945
R_1, wR_1 (all data)	0.0433, 0.1167
min/max $\Delta\rho$, e Å^{-3}	−2.463/1.264

[a] $\omega = 1/[s^2(F_o^2) + (0.0613P)^2 + 0.2174P]$, where $P = (F_o^2 + 2F_c^2)/3$.

Table 2. Selected Bond Distances and Angles of $Cs_2HgCl_2I_2$

bond	bond length (Å)	bond	bond angle (deg)
Hg1−Cl(1)	2.615(7)	Cl(2)−Hg−Cl(1)	92.99(6)
Hg1−Cl(2)	2.582(7)	Cl(2)−Hg−I(2)	106.25(19)
Hg1−I(2)	2.6882(8)	Cl(1)−Hg−I(2)	104.39(18)
Hg1−I(1)	2.6889(8)	Cl(2)−Hg−I(1)	105.39(19)
		Cl(1)−Hg−I(1)	106.03(18)
		I(2)−Hg−I(1)	134.27(3)

dx.doi.org/10.1021/ja3037299 | J. Am. Chem. Soc. 2012, 134, 14818−14822

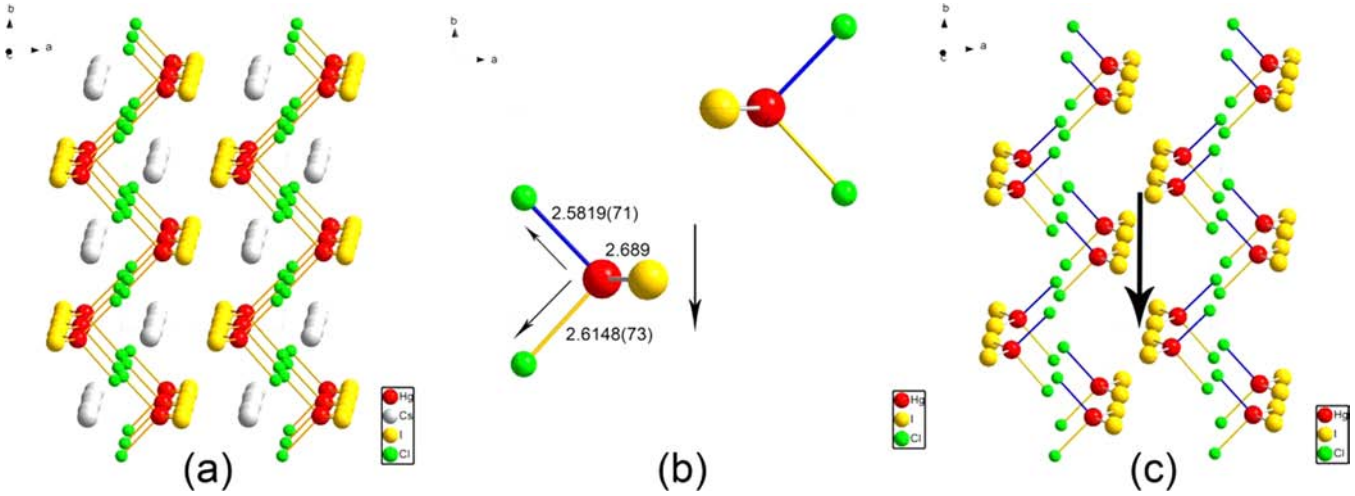

Figure 1. (a) Ball-and-stick diagram of $Cs_2HgI_2Cl_2$. (b) Ball-and stick diagram of $HgCl_2I_2$ tetrahedron in a unit cell. Each Hg atom is bonded to two iodine atoms with the same distance and two chlorine atoms with different distances (the shorter Hg−Cl bond is in blue and the longer one in yellow), giving rise to a net dipole moment antiparallel to the *b* direction (indicated by the black arrow). (c) Ball-and-stick diagram of $Cs_2HgI_2Cl_2$ crystal (Cs atoms are omitted for clarity). The shorter Hg−Cl bonds (in blue) are always located above the Hg atoms in each $HgCl_2I_2$ tetrahedron, giving rise to a net dipole moment antiparallel to the *b* axis (indicated by the large black arrow).

endured gradually enhanced radiation until their appearance changed under a magnifier after the irradiation.

Thermogravimetric Analysis. The thermogravimetric analysis (TGA) was carried out on Setaram SETSYS-16 simultaneous analyzer instrument. The crystal sample was added into an Al_2O_3 crucible and heated from room temperature to 800 °C at a heating rate of 10 K/min under flowing nitrogen gas.

RESULTS AND DISCUSSION

Crystal Structure. Single-crystal X-ray diffraction data for $Cs_2HgI_2Cl_2$ is presented in Table 1. It belongs to monoclinic structure with a noncentrosymmetric space group, $P2_1$. Its cell parameters are a = 8.0095(12) Å, b = 7.7557(12) Å, c = 9.8426(14) Å, β = 108.160(2)°, Z = 2, and V = 580.96(15) Å ^{3}. Selected bond lengths and angles are listed in Table 2.

Figure 1 shows the ball-and-stick diagrams of $Cs_2HgI_2Cl_2$. Each $(HgCl_2I_2)^{2-}$ group forms an isolated and distorted tetrahedron (Figure 1b), which is connected with its neighbors to form a chain along the *c*-axis. The chains are then connected each other to form layers along the *bc* plane, and the planes are further connected into a three-dimensional framework by the Cs atoms that occupy the empty spaces surrounded by halide atoms (Figure 1a). As shown in Figure 1b, there are two types of Hg−Cl bond lengths, but the same bond length for two Hg−I bonds. The Hg−Cl [2.5819(71)−2.6148(73) Å] bond lengths are slightly longer than those (2.438−2.540 Å) in Cs_3HgCl_5,[36] and the Hg−I [2.689 Å] distance is slightly shorter than those (2.738−2.819 Å) in Cs_2HgI_4.[37] The shorter Hg−Cl bonds are marked in blue and the longer one in yellow (see Figure 1b). Interestingly, all the shorter Hg−Cl bonds are located above the Hg atoms in each $HgCl_2I_2$ tetrahedron (Figure 1b,c). This packing style gives rise to a net polarization antiparallel to the direction of the *b* axis (indicated by the larger black arrow in Figure 1c). It is due to this net polarization that we observe the substantial SHG response.

Optical Properties . The ATR-FTIR spectrum and Raman spectrum of $Cs_2HgI_2Cl_2$ crystalline samples are shown in Figures 2 and 3, respectively. The ATR-FTIR spectrum shows no absorption in the middle IR region from 4000 to 700 cm^{-1} (2.5−14 μm). The Raman spectrum was collected in the region

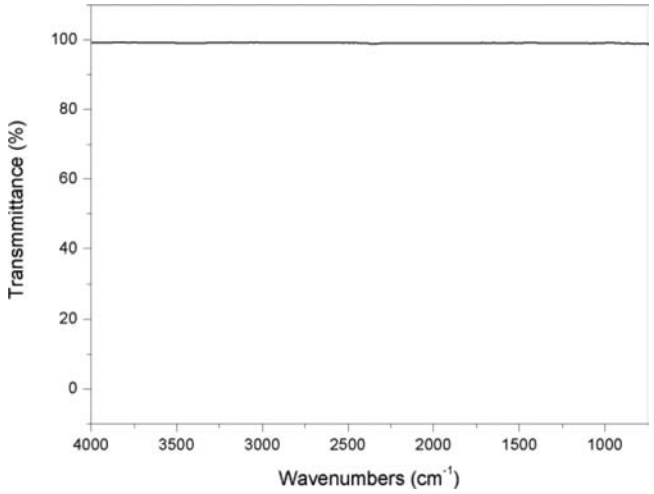

Figure 2. ATR-FTIR spectrum of $Cs_2HgI_2Cl_2$ crystal.

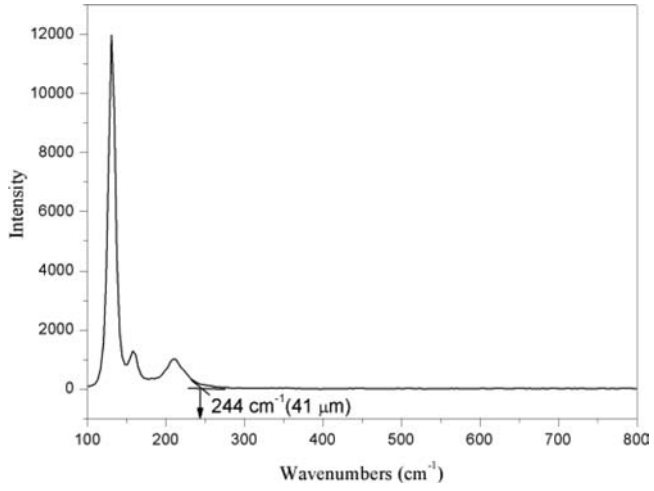

Figure 3. Raman spectrum of $Cs_2HgI_2Cl_2$ crystal.

dx.doi.org/10.1021/ja3037299 | J. Am. Chem. Soc. 2012, 134, 14818−14822

from 800 to 100 cm^{-1}(12.5−100 μm). There is no absorption in the region from 800 to 244 cm^{-1}(12.5−41 μm). These facts indicate that the transparency edge of $Cs_2HgI_2Cl_2$ reaches 41 μm at far-IR side. The UV−vis diffuse reflectance spectrum for $Cs_2HgI_2Cl_2$ is shown in Figure 4. The compound is colorless,

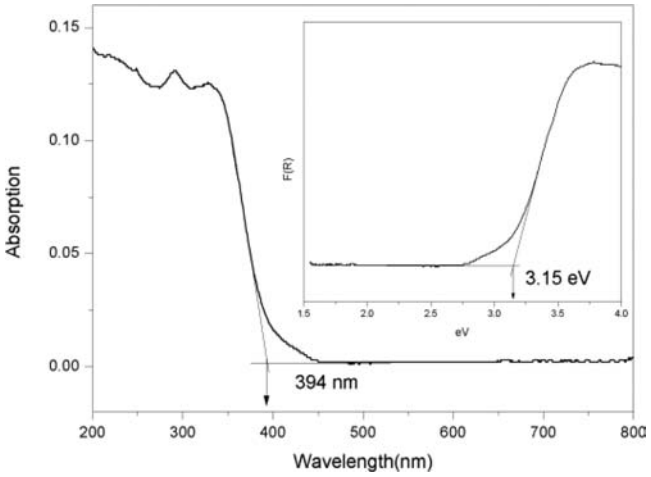

Figure 4. UV−vis spectrum of $Cs_2HgI_2Cl_2$ microcrystalline sample.

the spectrum shows that the absorption edge near the UV side is at about 394 nm, and this indicates that the band gap of the compound is approximately 3.15 eV. Based on these data, the transparent range of $Cs_2HgI_2Cl_2$ is 0.4−41 μm.

NLO Property and LDT Measurements. Powder SHG measurements using 1064 nm radiation revealed that $Cs_2HgI_2Cl_2$ showed SHG efficiencies as strong as KDP. Study of the SHG intensity as a function of particle size (from 40 to 200 μm) is shown in Figure 5. The intensity of the SHG signals

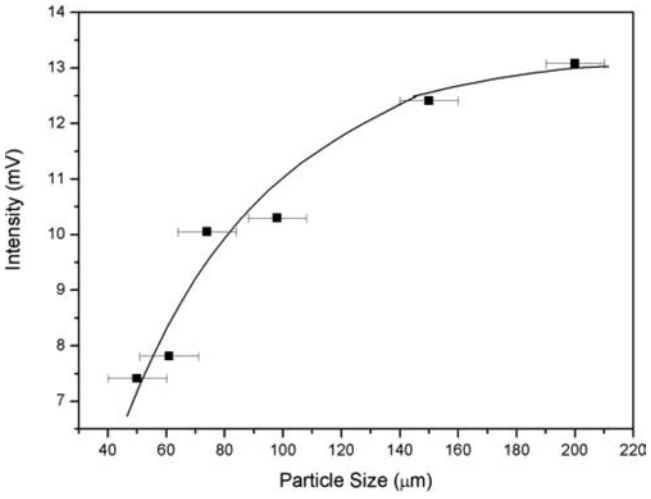

Figure 5. Dependence of SHG intensity on the particle size.

at first increases gradually with the increase of the sample size. And then it reaches a plateau at the maximum value after a certain particle size (of about 150 μm), which is a clear sign that the SHG of $Cs_2HgI_2Cl_2$ is phase-matchable.[35] These experimental results are also confirmed by the first-principles plane-wave pseudopotential methods,[38−40] which have been successfully applied in many IR NLO crystals.[41,42] The calculated static SHG coefficients for $Cs_2HgI_2Cl_2$ are d_{21} = −0.25 pm/V, d_{36} = 0.10 pm/V, and d_{22} = −0.37 pm/V. In addition, the very large birefringence of the $Cs_2HgCl_2I_2$ crystal is predicted as 0.198 at the wavelength of 1064 nm and 0.184 at 2090 nm. The large optical anisotropy can be understood from the microscopic structural features of the $(HgCl_2I_2)^{2-}$ group. Namely, the asymmetrical Hg−Cl and Hg−I bonds significantly increase the anisotropy and polarity of the dipole moment in the anionic group.

A preliminary examination of the laser-induced damage threshold has been carried out on small crystalline samples with a Q-switched laser source. The samples showed a damage threshold of about 83 MW/cm^2 (1064 nm, 5 ns). This value is higher than that of $AgGaS_2$ (AGS), and the latter is a commercially used IR NLO crystal with the LDT at about 30 MW/cm^2.[43]

Thermogravimetric Analysis. The thermal behavior of $Cs_2HgI_2Cl_2$ was investigated using thermogravimetric analysis (TGA). The compound is thermally stable up to 220 °C when it starts losing weight (Figure 6). From 220 to 460 °C, the

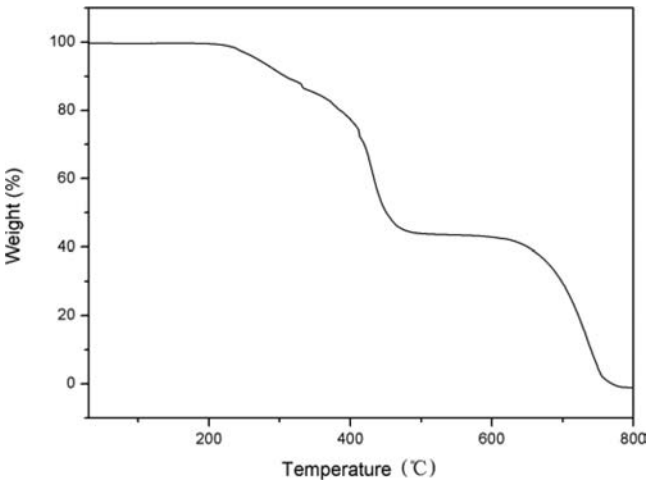

Figure 6. Thermogravimetric analysis curve for $Cs_2HgI_2Cl_2$ crystal.

compound continues to lose weight until about 44% remains. This implies that the residue is mainly CsCl (whose weight portion in $Cs_2HgI_2Cl_2$ is 42.6%). The colorless crystal is not hygroscopic.

CONCLUSION

In summary, $Cs_2HgI_2Cl_2$ single crystals can be obtained by the reaction in acetone. The intensity of the second harmonic generation effect is as strong as that of KDP, and the effect is phase-matchable, which is confirmed by the first-principles calculations. The compound is transparent in the range of 0.4−41 μm. A preliminary measurement indicates that its laser-induced damage threshold is quite high (about 83 MW/cm^2). Owing to these properties, $Cs_2HgI_2Cl_2$ appears to be a potential new NLO crystal applicable in the IR region.

ASSOCIATED CONTENT

Supporting Information

Powder X-ray diffraction pattern data and crystal data (CIF). This material is available free of charge via the Internet at http://pubs.acs.org.

AUTHOR INFORMATION

Corresponding Author

jgqin@whu.edu.cn; zslin@mail.ipc.ac.cn

Author Contributions

[⊥]These authors contributed equally.

Notes

The authors declare no competing financial interest.

■ ACKNOWLEDGMENTS

This work was supported by the National Science Foundation of China (Grant Nos. 91022036 and 11174297) and the National Key Fundamental Research (973) Program of China (Grant No. 2010CB630701). We thank Mr. Kuizhan Shao and Prof. Zhongmin Su of Northeast Normal University, China, for their help with the single-crystal structure analysis.

■ REFERENCES

(1) Burland, D. M.; Miller, R. D.; Walsh, C. A. *Chem. Rev.* **1994**, *94* (1), 31−75.
(2) Chai, B. H. T. Optical Crystals. In *CRC Handbook of Laser Science and Technology, Supplement 2: Optical Materials*; Weber, M. J., Ed.; CRC Press: Boca Raton, FL, 1995; pp 3−65.
(3) Chen, C.; Wu, B.; Jiang, A.; You, G. *Sci. Sin., Ser. B* **1985**, *28* (3), 235−243.
(4) Chen, C.; Wu, Y.; Jiang, A.; Wu, B.; You, G.; Li, R.; Lin, S. *J. Opt. Soc. Am. B* **1989**, *6* (4), 616−621.
(5) Smith, W. L. *Appl. Opt.* **1977**, *16* (7), 798.
(6) Kato, K. *IEEE J. Quantum Electron.* **1991**, *27*, 1137−1140.
(7) Boyd, G. D.; Miller, R. C.; Nassau, K.; Bond, W. L.; Savage, A. *Appl. Phys. Lett.* **1964**, *5* (11), 234−236.
(8) Okorogu, A. O.; Mirov, S. B.; Lee, W.; Crouthamel, D. I.; Jenkins, N.; Dergachev, A. Y.; Vodopyanov, K. L.; Badikov, V. V. *Opt .Commun.* **1998**, *155* (4−6), 307−312.
(9) Chemla, D. S.; Kupecek, P. J.; Robertson, D. S.; Smith, R. C. *Opt. Commun.* **1971**, *3* (1), 29−31.
(10) Boyd, G. D.; Kasper, H. M.; McFee, J. H.; Storz, F. G. *IEEE J. Quant .Electron.* **1972**, *QE-8* (12), 900−908.
(11) Boyd, G. D.; Buehler, E.; Storz, F. G. *Appl. Phys. Lett.* **1971**, *18* (7), 301−304.
(12) Zhang, K. C.; Wang, X. M. *Nonlinear Optical Crystal Materials*; Science Press: Beijing, 2005; pp 79−115.
(13) Nikogosyan, D. N. *Nonlinear Optical Crystals: A Complete Survey*; Springer: New York, 2005; pp 102−103.
(14) Zawilski, K. T.; Setzler, S. D.; Schunemann, P. G.; Thomas, M. P. *J. Opt. Soc. Am. B* **2006**, *23* (11), 2310−2316.
(15) Knippels, G. M. H.; van der Meer, A. F. G.; MacLeod, A. M.; Yelisseyev, A.; Isaenko, L.; Lobanov, S.; Thénot, I.; Zondy, J. J. *Opt. Lett.* **2001**, *26* (9), 617−619.
(16) Lin, X. S; Zhang, G.; Ye, N. *Cryst. Growth Des.* **2009**, *9* (2), 1186−1189.
(17) Shen, Y. R. *The Principles of Nonlinear Optics*; John Wiley & Sons, Inc.: New York, 1984; pp 1−200.
(18) Jackson, A. G; Ohmer, M. C.; LeClair, S. R. *Infrared Phys. Technol.* **1997**, *38*, 233−244.
(19) Zhang, J.; Su, N. B.; Yang, C. L.; Qin, J. G.; Ye, N.; Wu, B. C.; Chen, C. T. *Proc. SPIE* **1998**, *3556*, 1.
(20) Ren, P.; Qin, J. G.; Chen, C. T. *Inorg. Chem.* **2003**, *42*, 8−10.
(21) Liu, T.; Qin, J. G.; Zhang, G.; Zhu, T. X.; Niu, F.; Wu, Y. C.; Chen, C. T. *Appl. Phys. Lett.* **2008**, *93*, No. 091102.
(22) Zhang, G.; Qin, J. G.; Liu, T.; Li, Y. J.; Wu, Y. C.; Chen, C. T. *Appl. Phys. Lett.* **2009**, *95*, No. 261104.
(23) Chen, M. C.; Wu, L. M.; Lin, H.; Zhou, L. J.; Chen, L. *J. Am. Chem. Soc.* **2012**, *134* (14), 6058−6060.
(24) Yu, P.; Zhou, L. J.; Chen, L. *J. Am. Chem. Soc.* **2012**, *134* (4), 2227−2235.
(25) Yeon, J.; Kim, S. H.; Nguyen, S. D.; Lee, H.; Halasyamani, P. S. *Inorg. Chem.* **2012**, *51* (4), 2662−2668.
(26) Zhang, J. J.; Zhang, Z. H.; Sun, Y. X.; Zhang, C. Q.; Zhang, S. J.; Liu, Y.; Tao, X. T. *J. Mater. Chem.* **2012**, *22*, 9921−9927.
(27) Nguyen, S. D.; Yeon, J.; Kim, S. H.; Halasyamani, P. S. *J. Am. Chem. Soc.* **2011**, *133* (32), 12422−12425.
(28) Geng, L.; Cheng, W. D.; Lin, C. S.; Zhang, W. L.; Zhang, H.; He, Z. Z. *Inorg. Chem.* **2011**, *50* (12), 5679−5686.
(29) Sun, C. F.; Yang, B. P.; Mao, J. G. *Sci. China Chem.* **2011**, *54* (6), 911−922.
(30) Mei, D.; Yin, W.; Bai, L.; Lin, Z.; Yao, J.; Fu, P.; Wu, Y. *Dalton Trans.* **2011**, *40*, 3610−3615.
(31) Phanon, D.; Luneau, I. G. *Angew. Chem., Int. Ed.* **2007**, *46* (44), 8488−8491.
(32) Sheldrick, G. M. SHELXTL, version 6.14; Bruker Analytical X-ray Instruments, Inc., Madison, WI, USA, 2003.
(33) Sheldrick, G. M. *Acta Crystallogr.* **2008**, *A64*, 112−122.
(34) Wendlandt, W. M.; Hecht, H. G. *Reflectance Spectroscopy*; Interscience: New York, 1966; pp 62−65.
(35) Kurtz, S. K.; Perry, T. T. *J. Appl. Phys.* **1968**, *39*, 3798−3813.
(36) Clegg, W.; Brown, M. L.; Wilson, L. J. A. *Acta Crystallogr.* **1976**, *B32*, 2905−2906.
(37) Sjoevall, R.; Svensson, C. *Acta Crystallogr.* **1988**, *C44*, 207−210.
(38) Clark, S. J.; Segall, M. D.; Pickard, C. J.; Hasnip, P. J.; Probert, M. J.; Refson, K.; Payne, M. C. *Z. Kristallogr.* **2005**, *220*, 567−570.
(39) Chen, C. T.; Lin, Z. S.; Wang, Z. Z. *Appl. Phys. B: Lasers Opt.* **2005**, *80*, 1−25.
(40) In these calculations, generalized gradient approximation (GGA) with ultrasoft pseudopotentials were employed. We used a plane-wave cutoff of 500 eV, and a 3 × 3 × 3 special-*k*-point mesh for integrations over the Brillouin zones. The choice of these computational parameters ensures good convergence in present studies.
(41) Mei, D. J.; Yin, W. L.; Feng, K.; Lin, Z. S.; Bai, L.; Yao, J. Y.; Wu, Y. C. *Inorg. Chem.* **2012**, *51*, 1035−1040.
(42) Cao, Z. B.; Yue, Y. C.; Yao, J. Y.; Lin, Z. S.; He, R.; Hu, Z. G. *Inorg. Chem.* **2011**, *50*, 12818−12822.
(43) Chandra, S. ; Allik, T. H.; Catella, G.; Hutchinson, J. A. *Advanced Solid-State Lasers*; Bosenberg, W. R.; Fejer, M. M., Eds.; OSA Trends in Optics and Photonics Series, Vol. *19*; OSA: Washington, DC, 1998; pp 282−284.